Electron polarons and donor point defects in americium dioxide AmO_2

Martin S. Talla Noutack,* Michel Freyss,† and Gérald Jomard
CEA, DEN, DEC, Cadarache, F-13108 Saint-Paul-Lez-Durance, France

Grégory Geneste‡
CEA, DAM, DIF, F-91297 Arpajon, France

(Received 8 August 2019; published 22 January 2020)

Intrinsic donor point defects and electron polarons are investigated in bulk AmO_2 using density functional theory $+U$ calculations. Oxygen vacancies are deep double-donor defects, with transition energy levels closer to the valence band maximum than to the conduction band minimum. Americium interstitials are unlikely, due to prohibitive formation energies. Self-trapped electron polarons (which locally correspond to reducing one Am^{4+} in Am^{3+}) are found extremely stable (self-trapping energy $= -1.01$ eV). The electron is even more stable in the self-trapped state (far from an oxygen vacancy) rather than in association with an oxygen vacancy, indicating that oxygen vacancies have the tendency to spontaneously ionize, and thus automatically liberate electron polarons in the lattice. This large stability of the electron polarons confines the accessible range of Fermi levels to a very narrow interval between the valence band maximum E_{VBM} and $\sim E_{VBM} + 0.09$ eV. In oxygen-poor conditions, oxygen vacancies may be formed in rather large concentration in AmO_2 and have a strong probability to be doubly or singly ionized, with charge compensation being mostly ensured by a large number of electron polarons. The electron polaron hopping from an Am atom onto the nearest one involves a rather large activation energy of $\sim$0.6 eV and probably takes place by a nonadiabatic mechanism.

DOI: 10.1103/PhysRevB.101.024108

I. INTRODUCTION

Insulating metal oxides with partially filled f orbitals such as actinide oxides ($5f$), have a wide class of technological applications. For instance, americium oxides are considered as potential material for radioisotope thermoelectric generators for space exploration devices [1,2]. Furthermore, americium (a few percent) will be contained in the reference nuclear fuel envisaged for fast neutron reactors because it will be fabricated from uranium dioxide or mixed uranium-plutonium oxides spent fuel. The physical properties of these mixed oxides may thus be strongly influenced by those of americium oxides, especially AmO_2.

AmO_2 is an insulating oxide with a fluorite structure (like PuO_2 and UO_2) and a rather small band gap between 0.8 and 1.6 eV [3–6]. This material is known to undergo self-irradiation, namely α decay, which induces ballistic effects and related elastic collisions. This leads to atomic displacements, and thus damages such as lattice parameter expansion [7–9] and defect formation [10]. Self-irradiation damages in AmO_2 were the subject of very few studies in the literature. For instance, some authors have investigated the self-irradiation effect on structural properties of Am-bearing oxides using x-ray diffraction [11]. Furthermore, other authors have carried out studies on He bubbles and the nature of the defects induced by α decay in AmO_2 using transmission electronic microscopy [12]. However, no study to our knowledge has been undertaken on the elementary mechanisms occurring under self-irradiation in AmO_2, such as the formation and the migration of electronic and/or atomic point defects. Yet, a better knowledge of these mechanisms is essential to understand the evolution of the microstructure in this material.

Aside from the possible creation of point defects by self-irradiation effects (which is a nonequilibrium phenomenon), we note that the Am-O phase diagram has been shown to be rather complex. Americium oxides are mixed valence compounds, in which Am may exist in the two charge states +III (in Am_2O_3) and +IV (in AmO_2). There is a strong tendency for AmO_2 to the departure from stoichiometry, and the possibility of intermediate phases between AmO_2 and Am_2O_3 [13,14]. AmO_2 is thus a system that may easily deviate from the nominal O/Am ratio $= 2$, and in which oxygen vacancies are easily formed at equilibrium (thus independently from self-irradiation effects). In an ionocovalent insulator, any point defect (vacancy, interstitial, etc.) can generally be described either as an acceptor or as a donor. More explicitly, a defect releases holes or electrons, which can possibly be localized on one single atom (especially in the case of mixed valence), leading to a so-called small polaron. It is therefore strongly probable that oxygen vacancies in AmO_2 are associated with the presence of small electron polarons.

In this work, we investigate the chemistry of point defects in AmO_2. However, since AmO_2 is the most oxidized form of americium, which has, in most real conditions, the tendency to lose oxygen (yielding the appearance of Am^{3+}), the study of

*martin-stephane.tallanoutack@cea.fr
†michel.freyss@cea.fr
‡gregory.geneste@cea.fr

acceptor defects is not a relevant issue. We therefore restrict our investigations to native donor point defects, i.e., oxygen vacancies and americium interstitials, and to the behavior of excess electrons released in the lattice. Our computational approach is described in Sec. II. Section III presents the results on oxygen vacancies and americium interstitials. Some basic concepts about small polarons in insulators are briefly reviewed in Sec. IV before presenting the results on electron polaron in AmO_2 in Sec. V. Section VI establishes a simple defect model to discuss how our *ab initio* results can be used to estimate defect concentrations in AmO_2.

II. COMPUTATIONAL SCHEME

A. Defect formation energies

The formation energy of a point defect X in charge state q in AmO_2 is given by

$$\Delta E_f(X,q) = E_{\rm tot}(X,q) + E_{\rm corr} - E_{\rm tot}(AmO_2) - \sum_i \Delta n_i \mu_i + q\mu_e, \quad (1)$$

where $E_{\rm tot}(X,q)$ is the total energy of the AmO_2 supercell containing the defect X in charge state q and $E_{\rm tot}(AmO_2)$ is the energy of the supercell without defect (perfect system). $\Delta n_i = n_i$ (in defective system) (n_i in perfect system) denotes the variation in the number of atomic species i following the formation of the defect. μ_i is the chemical potential of species i. This variable reflects the external conditions in which the materials have been grown, i.e., i rich or i poor. μ_e is the electron chemical potential and $E_{\rm corr}$ is the set of corrections which are applied when the supercell is charged ($q \neq 0$).

The chemical potentials of Am and O cannot be completely determined through first-principles calculations because they depend on the external conditions (e.g., μ_O depends on temperature and oxygen partial pressure P_{O_2}), but knowledge of the stability domain of the AmO_2 oxide (with respect to other oxides and pure elements) provides an accessible range for these chemical potentials compatible with existence of bulk AmO_2. The formation enthalpy of AmO_2 writes

$$\Delta H_f^{AmO_2} = \mu_{AmO_2}^{\rm bulk} - \mu_{Am}^{Am_{met}} - 2\mu_O^{O_2} \quad (2)$$

with

$$\mu_{AmO_2}^{\rm bulk} = \mu_{Am} + 2\mu_O, \quad (3)$$

where $\mu_{Am}^{Am_{met}}$ is the Am chemical potential in its standard state (metallic α-americium), and $\mu_O^{O_2}$ is the O chemical potential in its standard oxygen gas state. We will now consider the chemical potentials of the elements with respect to their standard state:

$$\Delta\mu_{Am} = \mu_{Am} - \mu_{Am}^{Am_{met}}, \quad \Delta\mu_O = \mu_O - \mu_O^{O_2}. \quad (4)$$

In order to find the stability domain of AmO_2 with respect to O_2, α-Am and americium sesquioxide Am_2O_3, the following conditions should be satisfied:

$$\Delta\mu_O \leqslant 0, \quad \Delta\mu_{Am} \leqslant 0, \quad \Delta H_f^{AmO_2} = \Delta\mu_{Am} + 2\Delta\mu_O,$$
$$\Delta H_f^{Am_2O_3} \geqslant 2\Delta\mu_{Am} + 3\Delta\mu_O. \quad (5)$$

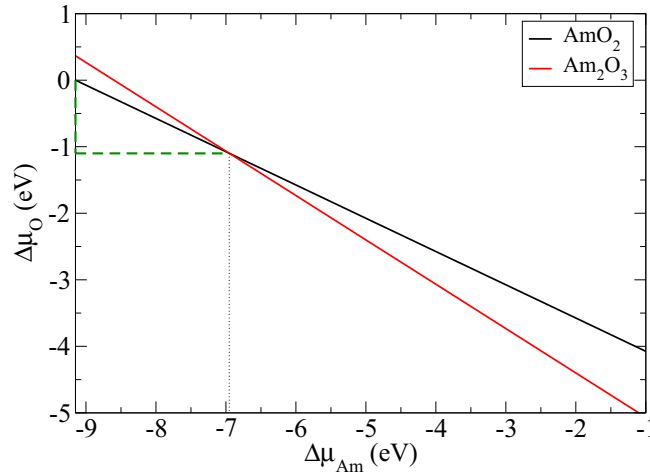

FIG. 1. $\Delta\mu_O$ as a function of $\Delta\mu_{Am}$ for different phases of the Am-O system. This figure is obtained by solving the set of Eqs. (5). For AmO_2 (respectively Am_2O_3), the formation enthalpies $\Delta H_f = -9.15$ eV (respectively -17.20 eV) are the ones obtained in our previous study [3] (see Table II).

For consistency, we take the GGA + U formation enthalpies as obtained in our previous work [3] $\Delta H_f^{AmO_2} = -9.15$ eV and $\Delta H_f^{Am_2O_3} = -17.20$ eV. The graphic solution of this set of equations is plotted on Fig. 1. From this figure, the accessible range for $\Delta\mu_{Am}$ and $\Delta\mu_O$ (in eV) regarding the stability of AmO_2 relative to Am_2O_3 and the pure elements in their standard state, write

$$-1.10 \leqslant \Delta\mu_O \leqslant 0, \quad (6)$$

$$-9.15 \leqslant \Delta\mu_{Am} \leqslant -6.95. \quad (7)$$

Since $\Delta\mu_{Am}$ and $\Delta\mu_O$ are related to each other by $\Delta H_f^{AmO_2} = \Delta\mu_{Am} + 2\Delta\mu_O$, the external conditions are completely fixed by choosing $\Delta\mu_O$ within the range of Eq. (6). Then, we have access to μ_{Am} and μ_O using Eq. (4). Density functional theory (DFT) total energies are used to estimate μ_i for O and Am in their standard state, i.e., $\mu_O^{O_2} = \frac{1}{2}E_{O_2}^{\rm tot}$ and $\mu_{Am}^{Am_{met}} = E_{\alpha\text{-Am}}^{\rm tot}$. However, the generalized gradient approximation (GGA), which is used in this work, is known to overestimate the binding energy of the O_2 molecule by about 1 eV. To overcome this problem, the total energy of the oxygen atom is used instead, and combined with the experimental value for the binding energy $E_{O_2}^{\rm coh}$ as follows:

$$2\mu_O^{O_2} = 2E_O^{\rm tot} + E_{O_2}^{\rm coh}, \quad (8)$$

where $E_{O_2}^{\rm coh}$ (<0) is the experimental binding energy of O_2 [15]. For consistency, the AmO_2 and Am_2O_3 formation enthalpies also include this correction [3].

In this study, we will consider two limiting cases which correspond to different external conditions, i.e. either O-rich or O-poor. The maximal value allowed for $\Delta\mu_O$ is 0. However, this oxygen chemical potential is in practice unreachable since it corresponds to extremely high oxygen pressure or very low temperatures: using ideal gas law [16] we find that $\Delta\mu_O = 0$ corresponds to $T = 300$ K and $P_{O_2} \sim 1.0 \times 10^9$ atm or $T \sim$ a few K and $P_{O_2} = 1.0$ atm. Thus, we use instead the ambient

TABLE I. External conditions (O-poor and O-rich) considered in this work.

	O-poor	O-rich
$\Delta\mu_O$	−0.75	−0.29
$\Delta\mu_{Am}$	−7.65	−8.56

conditions $T = 300$ K and $P_{O_2} = 0.2$ atm to define our O-rich conditions. This corresponds to $\Delta\mu_O = -0.29$ eV.

From Eq. (6), the minimal value allowed for $\Delta\mu_O$ is −1.10 eV. However, using such a value for $\Delta\mu_O$ leads to a situation in which the formation energies of neutral vacancies are very close to zero (∼0.04 eV). Moreover, combined with the formation energies of the electron polaron presented below, we would obtain that there is no region of the band gap over which all the defect formation energies would be positive. This apparent inconsistency disappears only for $\Delta\mu_O \gtrsim -0.93$ eV. In other words, there is a small interval of the chemical potential [−1.10; −0.93] eV over which either oxygen vacancies or electron polarons (or both) have a negative formation energy, and thus spontaneously form in very large quantity, leading to the loss of the AmO_2 compound integrity and the appearance of a large concentration of Am^{3+}. And yet AmO_2 should be more stable than Am_2O_3 over this interval of $\Delta\mu_O$ according to the formation enthalpies given above.

An explanation for this inconsistency is the possible existence of a phase with intermediate stoichiometry between AmO_2 and Am_2O_3, in relation with the easy departure from stoichiometry in AmO_2. As noticed in the Introduction, the Am-O phase diagram as determined experimentally is rather complex [13,14]. In particular, a phase with stoichiometry $AmO_{1.62}$ is reported in the experimental literature at high temperature, with a complex cubic structure [14,17], probably isostructural to C-type Am_2O_3. This phase should contain americium in both oxidation states Am^{3+} and Am^{4+}, and is probably stable for oxygen chemical potentials intermediate between those that stabilize Am_2O_3 and AmO_2. Considering this intermediate phase can explain why oxygen vacancies and/or electron polarons are found to spontaneously form in AmO_2 (and thus do exist in very large concentration) for $\Delta\mu_O \in [-1.10\text{ eV}; -0.93\text{ eV}]$.

As O-poor conditions, we will thus consider the following conditions: $\Delta\mu_O = -0.75$ eV, which corresponds to $T \sim 680$ K and $P_{O_2} = 0.2$ atm. The external conditions chosen to plot the defect formation energies in this work are summarized in Table I.

The formation energy of the electron polaron is defined as

$$\Delta E_f(e',\ -1) = E_{\text{tot}}(AmO_2 + e',\ -1) - E_{\text{tot}}(AmO_2) - \mu_e, \tag{9}$$

where $E_{\text{tot}}(AmO_2 + e',\ -1)$ is the total energy of the supercell containing one self-trapped electron polaron.

The calculation of defect formation energies according to Eq. (1) involves a correction term E_{corr}, which is the sum of the monopole part of the Markov-Payne correction [18] (using the static dielectric calculated in our previous work, see Table II) and of a band alignment performed using the 6*s* semicore levels of americium, as in Refs. [19,20]. In the case of the charged supercell containing a delocalized electron or a delocalized hole, however, only the band alignment correction is applied.

The electron chemical potential μ_e is referenced to the valence band maximum (VBM), E_{VBM}, and is written as $\mu_e = E_{\text{VBM}} + \epsilon_F$. The Fermi level ϵ_F is assumed to vary between 0 and the band gap E_g, equal to 1.1 eV (Table II) using $U = 6$ eV and $J = 0.75$ eV (Kohn-Sham band gap).

The energy of the VBM is calculated by [21] $E_{\text{VBM}} = E_{\text{tot}}(AmO_2) - E_{\text{tot}}(AmO_2, +1)$, with $E_{\text{tot}}(AmO_2, +1)$ being the energy of a perfect supercell in which an electron has been removed (thus emptying a delocalized Kohn-Sham state at the VBM). Also, we can estimate the energy of the conduction band minimum (CBM) in the same way, $E_{\text{CBM}} = E_{\text{tot}}(AmO_2, -1) - E_{\text{tot}}(AmO_2)$, with $E_{\text{tot}}(AmO_2, -1)$ being the energy of a perfect supercell in which an electron has been added (thus filling a delocalized Kohn-Sham state at the CBM). The band gap may then be alternatively obtained as $E_{\text{CBM}} - E_{\text{VBM}}$ and is found here to be 1.10 eV, thus very close to the Kohn-Sham band gap.

TABLE II. Lattice parameter, band gap, formation enthalpy, Am magnetic moment, and static dielectric constant ϵ_S of AmO_2 and Am_2O_3 obtained in our previous study and compared with other studies. Our results were obtained using GGA + U with $U = 6$ eV and $J = 0.75$ eV [3].

		a (Å)	Band gap (eV)	H_f (eV)	μ_{mag} (μ_B)	ϵ_S
AmO_2	GGA + U[a]	5.44	1.1	−9.15	5.1[b]	16.8
	Other works	5.42[c]; 5.37[d]	0.8[c]; 1.3[e]	−9.66[f]	4.8[g]	
Am_2O_3	GGA + U[a]	11.18	1.25	−17.20	6.2	
	Other works	11.02[d]		−17.52[e]		

[a]Previous work [3].
[b]Using 5f occupation matrices and no symmetry (5.2 from integration of electron density inside PAW atomic spheres) [3].
[c]Reference [6].
[d]Reference [9].
[e]Reference [5].
[f]Reference [34].
[g]Reference [35].

B. Density functional theory calculations

1. DFT functionals

Our DFT calculations are carried out using the ABINIT package [22,23] within the projector augmented wave (PAW) [24,25] formalism. We use the generalized gradient approximation, as parametrized by Perdew, Burke, and Ernzerhof (GGA-PBE) [26]. The strong correlations among the $5f$ electrons of americium are treated by adding an onsite Coulomb repulsion, under the form of a Hubbard-type term in the Hamiltonian [27]. The rotationally invariant form by Liechtenstein *et al.* [28] is used for the electron interaction energy associated with the Hubbard term (E_{Hub}). The total energy in this GGA + U scheme is the sum of the GGA energy (E^{GGA}), the Hubbard interaction energy E_{Hub} and the double-counting term E_{dc}:

$$E^{\mathrm{GGA}+U} = E^{\mathrm{GGA}} + E_{\mathrm{Hub}} - E_{\mathrm{dc}}. \tag{10}$$

For the double-counting expression (E_{dc}), we use the full localized limit (FLL) [27,29,30] because americium oxides have an insulating ground state (thus, orbital occupation of the strongly correlated $5f$ electrons is close to one or zero).

2. Numerical parameters

The onsite Coulomb terms U and J used for Am $5f$ orbitals are (6.00; 0.75) eV. Indeed, in our previous study [3], by computing several bulk properties of AmO_2 as a function of the U and J parameters and comparing with available experimental data, we showed that ($U = 6.00$; $J = 0.75$) eV can be used to provide a good description of AmO_2. Results are obtained using a plane-wave cutoff energy of 871 eV. According to our convergence tests, this parameter leads to a precision lower than 1 meV per atom on physical energies (total energy differences). A 96-atom supercell ($2 \times 2 \times 2$ in terms of the conventional fcc fluorite unit cell of AmO_2) is used, with various point defects inserted inside: oxygen vacancy, americium interstitial, and electron polaron.

The calculations are done using a $2 \times 2 \times 2$ k-point mesh to sample the Brillouin zone associated with the supercell, generated by the Monkhorst-Pack [31] method, which is sufficient for an energy convergence much better than 0.3 meV per atom on the insulating supercells. In the case of the metallic supercells (delocalized electron, delocalized hole), however, the k-point mesh is increased to $4 \times 4 \times 4$. We performed structural optimizations keeping fixed the lattice vectors (fixed according to the theoretical values yielded by GGA + U on bulk AmO_2) of the supercell, until the forces acting on the atoms become less than 2.0×10^{-4} Ha/bohrs ($\sim$0.01 eV/Å). In other words, only atomic positions are relaxed.

The supercell is constructed by doubling in the three directions the unit cell obtained in our previous work [3] after full structural relaxation without accounting for symmetries. Accordingly, the $5f$ occupation matrix denoted as $M_3^{\mathrm{no\,sym}}$ in Ref. [3] is used throughout this work to initialize all the supercell calculations. For the simulation of the electron polaron, however, a specific methodology is applied (see Sec. V). Note that a careful control of the occupation matrices of the $5f$ orbitals of americium is absolutely necessary to obtain a correct description of the ground state of the defective supercells within DFT + U, in order to avoid convergence toward electronic metastable states [32].

For the charged supercells, the extra charge is compensated by a uniform background, as usually done for the compensation of charged defects in insulator compounds. Oxygen vacancies are studied in charge states $q = 0, +1, +2$, americium interstitials in charge states $q = 0, +1, +2, +3$, and $+4$, and the electron polaron is simulated by adding an extra electron in the supercell ($q = -1$).

3. Magnetic configuration

All the present calculations are spin polarized, and symmetries are switched off. The 1k antiferromagnetic (AFM) state is assumed for AmO_2 since we showed in our previous study [3] that, although the magnetic ground state of AmO_2 is more probably a 3k AFM order below the Néel temperature (8.5 K), 1k AFM order (without taking relativistic effects into account) can be used as a good approximation. Thus, we do not include spin-orbit coupling (SOC) in our calculations, and perform all our calculations in the framework of collinear magnetism (i.e., the magnetization is a scalar field) with a 1k AFM order. Note that taking SOC into account is computationally extremely demanding, and prevents the use of supercells sufficiently large for an accurate description of the properties of defective systems. Furthermore, it has been showed in UO_2 [33] that the order of magnitude of energy corrections due to SOC is of the 10th electron volts, whereas defect formation energies are usually much larger (of the order of electron volts).

Table II gathers quantitative data on AmO_2 and Am_2O_3 compounds obtained in our previous study [3] and used throughout this study.

III. OXYGEN VACANCIES AND AMERICIUM INTERSTITIALS

We begin by a description of the donor point defects in AmO_2, i.e., oxygen vacancies and Am interstitials.

A. Oxygen vacancies

The oxygen vacancy is double-donor defect. It liberates two electrons. In its charge-neutral state (V_{O}^{X}), these two extra electrons are localized on two of the four adjacent Am atoms, giving rise to the formation of two Am^{3+} ions in the close vicinity of the vacancy. If these two electrons unbind from the vacancy and migrate far away in the lattice, they leave behind a charged (ionized) oxygen vacancy $V_{\mathrm{O}}^{\bullet\bullet}$ or at least a partially ionized oxygen vacancy $V_{\mathrm{O}}^{\bullet}$ if one of the electrons remains bonded to the vacancy. Indeed, the calculation of $V_{\mathrm{O}}^{\bullet}$ provides only one Am^{3+}, while the fully ionized oxygen vacancy $V_{\mathrm{O}}^{\bullet\bullet}$ is associated with no Am^{3+} in the supercell. Note that Am^{3+} are easily identified by their spin magnetic moment: our GGA + U calculations provide a moment of $\sim 5.8\,\mu_B$ for Am^{3+} versus $\sim 5.1\,\mu_B$ for Am^{4+} (in this work, the magnetic moments are evaluated using the $5f$ occupation matrices on Am atoms).

Figure 2 displays the formation energies of the oxygen vacancies V_{O}^{X}, $V_{\mathrm{O}}^{\bullet}$, and $V_{\mathrm{O}}^{\bullet\bullet}$ as a function of Fermi level in the two external conditions described above: oxidizing (O-rich) and reducing (O-poor). From these formation energies, we can

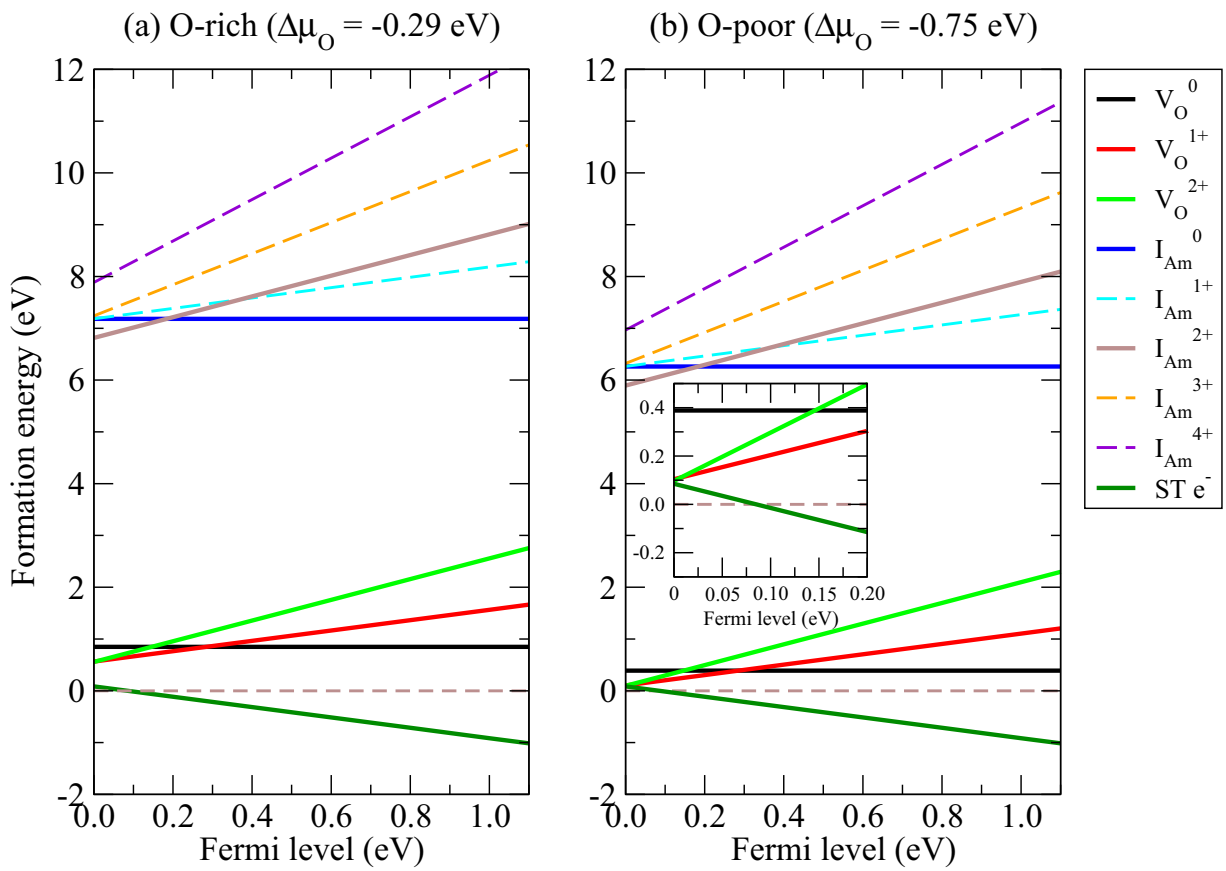

FIG. 2. Formation energies of the oxygen vacancy, americium interstitial, and self-trapped electron polaron in their possible charge states, as a function of the Fermi level in the band gap of AmO_2 for (a) oxygen-rich and (b) oxygen-poor conditions. ST e^- denotes the self-trapped electron polaron. Inset (in right panel): zoom on the VBM region.

calculate the transition energy level between the O vacancy in charge state q and the same defect in charge state q'. It is defined as

$$\epsilon_{V_O}(q/q') = \frac{\Delta E_f(V_O, q; \epsilon_F = 0) - \Delta E_f(V_O, q'; \epsilon_F = 0)}{q' - q}, \tag{11}$$

where $\Delta E_f(V_O, q; \epsilon_F = 0)$ is the formation energy of the O vacancy in charge state q, calculated for the Fermi level at the VBM [36]. $\epsilon_{V_M}(q/q')$ corresponds to the Fermi level at which the formation energies of the defect in charge states q and q' are equal.

We find here $\epsilon_{V_O}(+2/+1) = 0.01$ eV and $\epsilon_{V_O}(+1/0) = 0.28$ eV. These transition levels are very far from the CBM (~1 eV or more), indicating that the oxygen vacancy in AmO_2 is a *deep double-donor defect*.

Figures 3(d)–3(f) display the electronic density of states (e-DOS) of the supercell containing the charge-neutral oxygen vacancy. Figure 3(d) plots the total e-DOS. It can be seen that two occupied states with opposite spin appear in the band gap, but at very low energy, very close to the VBM (they are spotted with green arrows), which emphasizes the picture of a *deep donor* for the O vacancy in AmO_2. Figure 3(e) plots the e-DOS projected on the $5f$ orbitals of the two Am^{3+} which are next to the vacancy and that carry the two electrons released by the defect, while Fig. 3(f) plots the e-DOS projected on the $5f$ orbitals of two Am^{4+} (with opposite spin) of the supercell (their projected e-DOS are typical of those of the other Am^{4+}). We observe that the occupied $5f$ orbitals of Am^{4+} are localized down in the valence band, a feature that has already been pointed out in our previous work [3]. This positioning is noticeably changed for Am^{3+} since adding one electron in a $5f$ orbital has two effects: first, the energy of the newly occupied state strongly decreases from the CBM down to the VBM and, second, at the same time, the energy of the other $5f$ states increases towards the VBM.

Am^{3+} has thus the tendency to accumulate the occupied $5f$ states at the VBM, which can be seen as a precursor to the formation of Am_2O_3, which is a Mott insulator with a band gap Am $5f \rightarrow$ Am $5f$ (in contrast to AmO_2 which rather behaves as a charge-transfer insulator with a band gap O $2p \rightarrow$ Am $5f$).

B. Americium interstitials

The americium interstitial I_{Am} liberates four electrons and is thus a quadruple donor defect. In the charge-neutral state, I_{Am}^{X} induces the formation of four trivalent americium Am^{3+} in the crystal. Upon charging the defect, the number of Am^{3+} in the supercell decreases accordingly (3 for $I_{Am}^{\bullet}$, 2 for $I_{Am}^{\bullet\bullet}$, 1 for $I_{Am}^{\bullet\bullet\bullet}$) up to the fully ionized Am interstitial $I_{Am}^{\bullet\bullet\bullet\bullet}$, that does not induce the presence of any Am^{3+}, as expected.

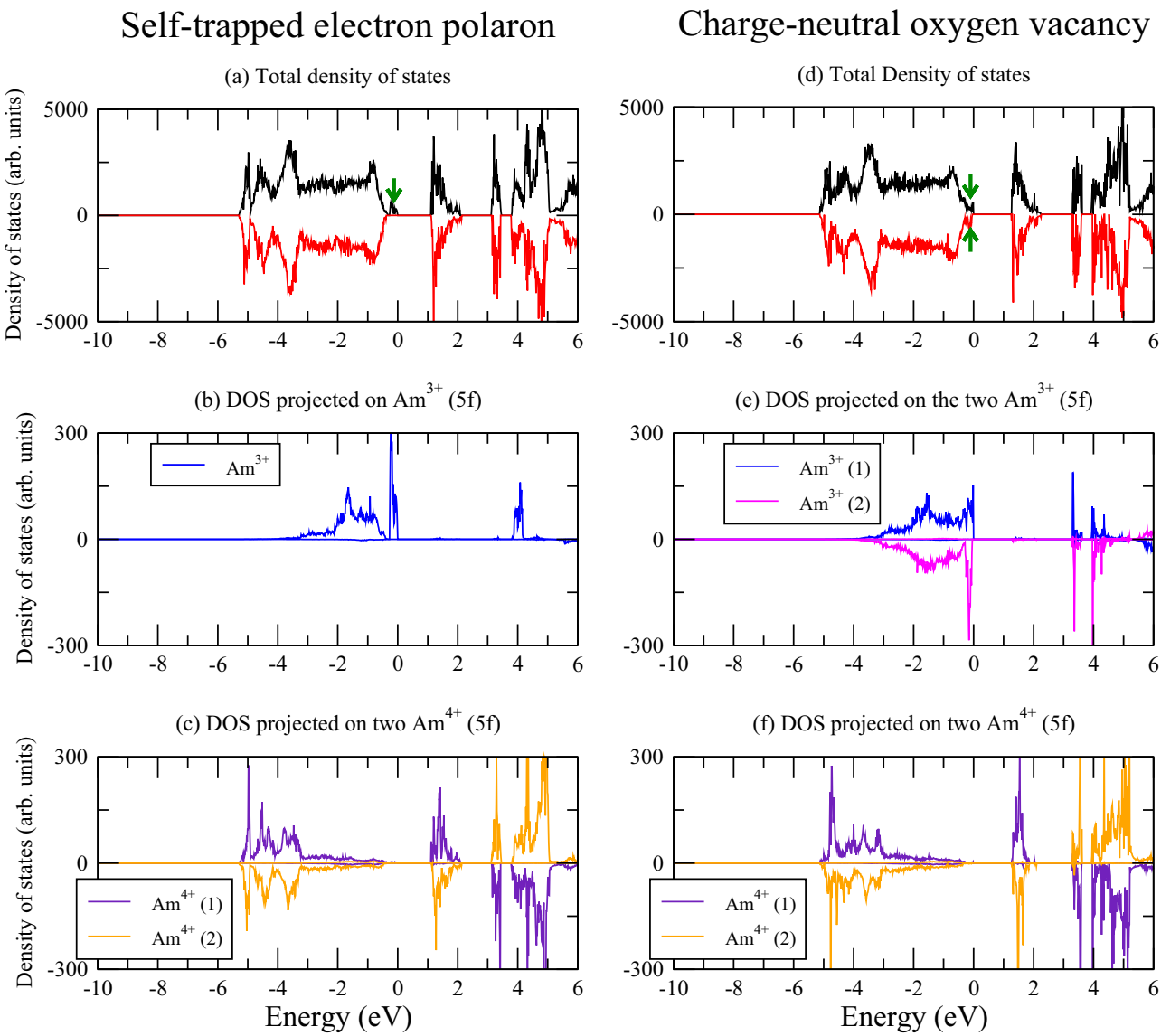

FIG. 3. Electronic density of states. Left panels: supercell with the self-trapped electron polaron. Right panels: supercell with the charge-neutral oxygen vacancy. Top: total density of states. Middle: density of states projected on f orbitals of the Am^{3+} atoms of the supercell (one single in the case of the polaron, two in the case of the vacancy). Bottom: density of states projected on f orbitals of two Am^{4+} with opposite spin of the supercell. In (a) and (d), the small green arrows spot the defect states (occupied in both cases). The Fermi energy (highest occupied state) is set at 0 eV. Positive values: spin up; negative values: spin down.

The formation energies of this defect in charge states q from 0 to +4 are plotted as a function of Fermi level on Fig. 2, superimposed to those of the oxygen vacancy. Only two of the studied charge states are found stable: $I^{\bullet\bullet}_{\mathrm{Am}}$ and I^{X}_{Am}, with a transition energy level between them equal to $\epsilon_{I_{\mathrm{Am}}}(+2/0) = 0.18$ eV. Once again, this ionization energy is far from the CBM, which indicates that the Am interstitial is a deep donor, as the oxygen vacancy.

On the other hand, one can see (Fig. 2) that the formation energies of Am interstitials are several eV higher ($\sim$6 eV at $\epsilon_F = 0.0$ eV) than those of the oxygen vacancies, indicating that these defects are unlikely, and will never be present in the AmO_2 matrix. This suggests that the majority of the intrinsic donor defects in AmO_2 are the oxygen vacancies.

IV. SELF-TRAPPED SMALL POLARONS IN INSULATORS: BASIC CONCEPTS

Having described the donor point defects in AmO_2, we now investigate how the electrons released by these defects behave in the lattice and, more precisely, whether they can localize on single Am atoms far from the vacancies, under the form of small polarons. Before, however, we briefly review some basic concepts about small polarons in insulators.

A. Self-trapping

A small polaron corresponds to the localization of an extra elementary electronic charge (electron or hole) on a single atom in an insulating crystal, associated with a set of atomic distortions around. In an insulator, these charges

are generally released by some point defect. For example, in most oxide materials, the oxygen vacancy liberates two electrons. These two electrons can either stay localized very close to the vacancy (which is then said to be in the neutral state), or diffuse in the lattice, leaving behind them a doubly charged oxygen vacancy. Whether the vacancy is ionized or not depends on the electronic chemical potential μ_e. If one of these electrons, once released in the lattice, localizes on a single atom, the entity corresponding to this localized electron, with the associated lattice distortion is called a *small polaron*.

The mechanism by which an extra electronic charge localizes on a single atom in the lattice is called *self-trapping*: this is a self-consistent mechanism along which the localization of the electronic charge, and the appearance of distortions around it favor each other. Indeed, the localization of the electronic charge on one atom (which corresponds to a change in the oxidation state of the atom) creates a distortion all around because it breaks the translational periodicity of the lattice. Moreover, this distortion is mostly the result of the electrostatic interaction between the localized electronic charge and the surrounding polarizable matrix. The immediate environment is therefore radially polarized. In return, this polarization field creates on the polaronic site a deep electrostatic potential which favors the localization of the charge. Roughly speaking, the formation of a polaronic state (rather than a delocalized Bloch-type band state) takes place if the energy cost associated with the self-trapping distortion and the quantum confinement of the charge is compensated by the (favorable) interaction between the charge and the polarization field of the self-trapping distortion, a balance which is obviously system dependent. Other mechanisms (electron-electron interaction, stress field associated with the polaron) also play a role. It is important to understand that the charge localization and the self-trapping distortion are necessary to each other and cannot be dissociated in a small polaron. The formation of the polaronic state is schematically described on Figs. 4(a) and 4(b).

B. Diffusion

Under the effect of thermal fluctuations, small polarons may jump from an atom onto a nearest one. However, the physical mechanism that underlies this hopping is not the same as the one encountered in the hopping of (heavy enough) atoms. Indeed, atomic hopping is usually considered as resulting from a thermal overbarrier process (at least at large enough temperature), in which the potential energy barrier that separates one site from the other is overcome thanks to the thermal vibrations of the atoms themselves (including those of the hopping atom). In the case of small polaron hopping, however, it is not possible to invoke the thermal vibrations of the localized electron (or hole) itself because this charge carrier, in its ground state, is subject to a strong quantum confinement, associated to a strong quantization of its energy levels. At room or moderate temperatures, the excited states of the localized charge may lie too high, so that the localized charge, in many situations, does not undergo the thermal fluctuations and remains frozen in its ground state. Thus, the notion of thermal overbarrier for a localized electron (or hole), i.e., including the thermal fluctuations of the electron

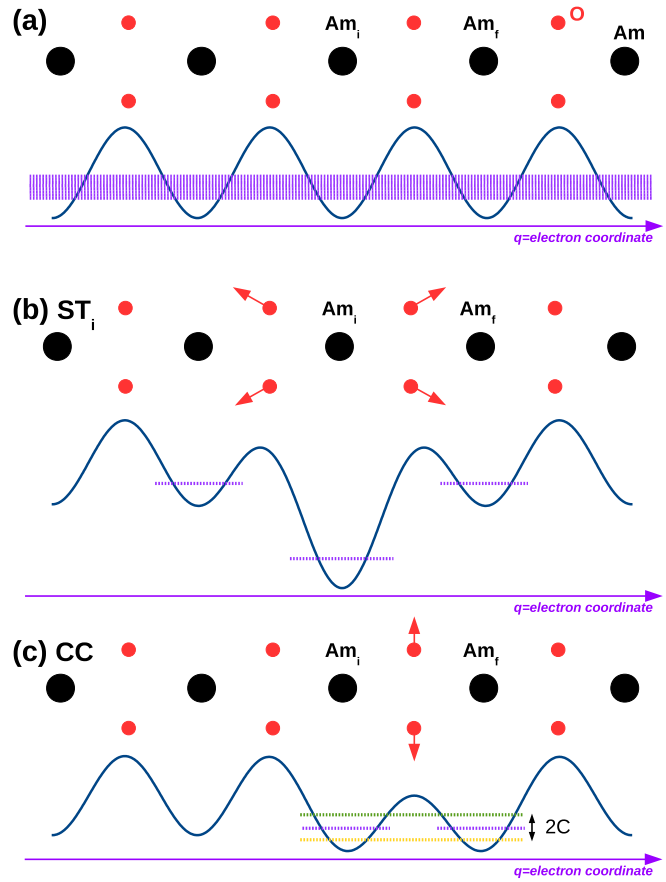

FIG. 4. Schematic representation of the self-trapping process [37] of an excess electron in AmO_2 (the positioning of Am and O atoms is here schematic and does not correspond to that of the real fluorite structure). The blue line schematically represents the potentiel felt by the electron; (a) periodic undistorted crystal: the excess electron is delocalized throughout the crystal under the form of a Bloch wave and its eigenstates form a band (purple lines); (b) self-trapped state at site Am_i: the crystal is distorted around the particle (here the first-neighbor oxygens are pushed away, which is schematically featured by the red arrows), which makes the Am_i site more stable than the neighboring sites for the excess electron. Note that transfer by tunneling from Am_i site onto the neighboring sites is impossible. The polaron is the association of the particle localized at site Am_i and of the set of surrounding distortions; (c) coincidence configuration (CC) [37] for polaron hopping from site Am_i onto site Am_f: the atomic distortions have been modified so that the electron feels a symmetric potential, the two (diabatic) ground levels in the two wells (Am_i and Am_f) are equalized (purple lines), making transfer by tunneling possible through the remaining barrier. The green/yellow lines represent the ground and first-excited adiabatic states of the electron, which, at coincidence, are separated by $2C$ (electronic coupling).

(or hole) itself, does not make sense in such a situation. And yet, small polaron hopping is known as being a thermally activated process [38], with a hopping rate being proportional to an Arrhenius term e^{-E_c/k_BT}.

In fact, the process by which the small polaron hopping takes place involves thermal fluctuations, but those of the lattice atoms. With temperature, the atomic vibrations occurring

around the polaron may, occasionally, lead to specific atomic configurations in which the self-trapping is weakened and, more precisely, confined to a pair of neighboring sites (instead of one), so that the energy of the electronic charge is the same whether it is localized on the initial site or on the final site [see Fig. 4(c)]. Such an atomic configuration, in which the energies of the ground states in the initial well and in the final well are in coincidence, is called a coincidence configuration (CC) [37]. These specific lattice configurations are the ones in which the hopping of the excess electronic charge may effectively take place because they are favorable to a resonant tunneling between the two (diabatic, i.e., considered as constrained to remain localized on one site) ground states (the charge feels a symmetric double well at coincidence). The mechanism by which the electronic charge transfers onto the nearest site is thus intrinsically quantum (tunneling), but this tunneling takes place in a specific configuration created by the thermal fluctuations of the lattice atoms.

There is obviously an infinity of such coincidence configurations, and many of them can play a role in the hopping. However, very often in polaronic hoppings, one single coincidence configuration is relevant (that of lowest energy) [37]. It plays the role of the saddle point configuration for the polaronic hopping process. Let us call its energy E_c (with respect to the self-trapped state of the polaron). Since this configuration is reached by thermal fluctuations, the rate at which it is visited is therefore proportional to e^{-E_c/k_BT}, which explains the Arrhenius form of the polaronic hopping rate.

The reaction coordinate for the hopping of the polaron consists therefore in the set of atomic distortions that drives the system from the initial self-trapped configuration (denoted as ST_i) up to the final self-trapped one (denoted as ST_f), transiting along the path by the coincidence configuration (CC). Here, we denote this (atomic) reaction coordinate as S. The set of atomic distortions along S may follow one or several phonon modes of the lattice. For simplicity, we consider that only one phonon mode, with pulsation ω_S, contributes to the reaction coordinate S. $\frac{\omega_S}{2\pi}$ can therefore be considered as an attempt frequency for the hopping of the small polaron.

The energy of the system as a function of S is schematically plotted on Fig. 5. The dashed curves on this figure represent the energy of the system with an excess electron in its ground state, considered as strictly localized on the initial or on the final atom. They are often called *diabatic* curves (or diabatic surfaces) and, as explained above, they cross at CC. However, at coincidence, the two electronic diabatic ground states are usually coupled, and the electronic coupling C breaks the degeneracy, so that the two adiabatic levels (i.e., the true electronic eigenstates within the adiabatic approximation) are split by $2C$. Taking into account the coupling C, the energy of the system as a function of S is represented by the *adiabatic* curves (or adiabatic surfaces, solid lines on Fig. 5). Note that the adiabatic curves deviate from the diabatic ones only around the coincidence point

We have said that polaronic hopping takes place in a coincidence configuration, by a tunneling of the charge through the barrier felt at coincidence. Indeed, in a symmetric double well, a quantum particle initially localized in one of the two wells with an energy smaller than the barrier oscillates, through a tunneling motion, with a typical time $\hbar/2C$, where C is the

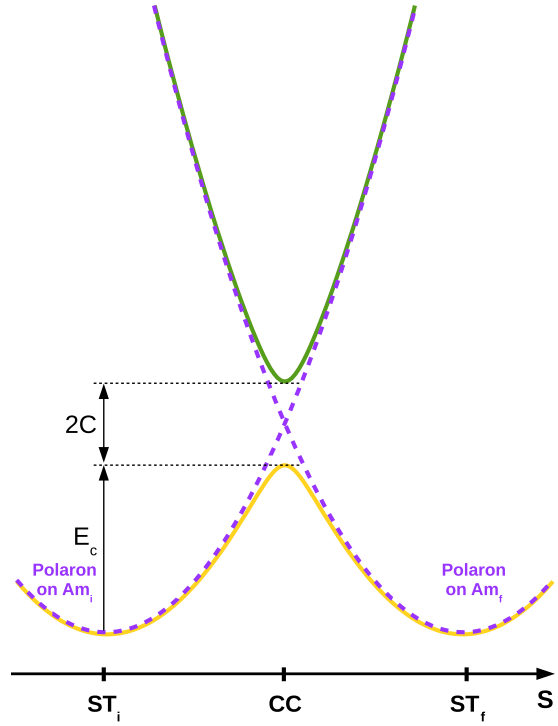

FIG. 5. Typical energy profile along the hopping path of a small electron polaron, as a function of the reaction coordinate, denoted here as S. S is an atomic distortion that drives the lattice from the initial self-trapped configuration (ST_i) to the final self-trapped one (ST_f), passing by a coincidence configuration at the transition point (CC). It is important to distinguish this energy profile (function of an atomic coordinate) from the ones drawn on Figs. 4(b) and 4(c), which correspond to the electronic potential (i.e., seen by the excess electron) at fixed lattice configuration (either ST_i or CC). E_c is the coincidence energy, which plays the role of the activation energy for the hopping process of the small polaron.

electronic coupling. $2C$ is the energy separation between the ground and first-excited (adiabatic) states in the double well at coincidence. However, the coincidence event has a certain timescale itself and, obviously, the hopping event does take place only provided the typical time for tunneling through the barrier is smaller than the coincidence timescale. Thus, two opposite limit behaviors may exist:

(i) If the typical time for tunneling through the barrier at coincidence is much smaller than the coincidence timescale, polaronic hopping is automatic at each coincidence event. In other words, it is as if the polaron had the time to adjust its state to the atomic configuration: the hopping is thus said to be adiabatic because the system stays on the adiabatic surface all along the transfer (the adiabatic approximation is always true). The hopping rate in that case takes the form $k = k_0 e^{-E_c/k_BT}$, k_0 being the typical frequency of the phonon mode that drives the system to the coincidence ($\sim 10^{13}$ s^{-1}).

(ii) If, on the contrary, the typical time for tunneling through the barrier at coincidence is much larger than the coincidence timescale, polaronic hopping is not automatic at all, and many occurrences of the coincidence configuration can be necessary before the jump takes place. The prefactor of the jump rate in that case is controlled, not only by the

phonons, but also by the probability for the charge to transfer through the barrier at coincidence, which is a typical quantum mechanism, and will involve the coupling C in the expression of the prefactor. The prefactor may in that case be much smaller than the phonon frequencies ($k_0 \ll 10^{13}\ s^{-1}$). In that case, since the polaronic charge has not the time to adjust its state to the atomic configuration and remains on one side of the symmetric barrier at coincidence (instead of adjusting to the true adiabatic ground state which is delocalized over the two wells), the jump is said to be nonadiabatic because the system leaves the adiabatic surface around CC (the adiabatic approximation is not true at CC).

Whether polaron transfer takes place adiabatically or not may be determined by inspecting the Landau-Zener adiabaticity criterion [38] (or Landau-Zener thermal parameter)

$$\gamma_{\text{th}}(T) = \frac{2\pi}{\hbar\omega_S}\sqrt{\frac{\pi}{E_S k_B T}}C^2, \tag{12}$$

in which ω_S is the pulsation of the lattice phonon mode that drives the system from the self-trapped configuration up to the coincidence, and E_S is the reorganization energy, that may be approximated by $4E_c$ in a harmonic model. Note that γ_{th} has been used also to characterize the adiabaticity of proton transfers in solutions [39].

$\gamma_{\text{th}} \gg 1$ corresponds to the adiabatic case, the prefactor of the transfer rate in then $k_0 = \frac{\omega_S}{2\pi}$. In contrast, $\gamma_{\text{th}} \ll 1$ corresponds to the nonadiabatic situation described above.

V. ELECTRON POLARON

The results of Sec. III clearly indicate that the donor defects in AmO_2 tend to form Am^{3+} cations thanks to the localization of the electrons released by the defect on single Am atoms. Note that this local change of oxidation state of americium is in agreement with the electronic density of states of AmO_2, for which the CBM has been shown to be formed by Am $5f$ states (see, e.g., our previous work [3]): the electrons released by the donor O vacancy thus come to populate these states, forming Am^{3+}.

However, instead of localizing on single atoms in the vicinity of the defect, the excess electrons can escape and diffuse through the crystal. Here, two limit behaviors are *a priori* possible: either they are delocalized, under the form of a Bloch wave [conduction electron, Fig. 4(a)], or they remain localized on another single Am atom, which corresponds therefore to a self-trapped electron polaron [Fig. 4(b)]. The mechanisms by which an electron can localize on a single atom far from a defect (self-trapping) have been recalled in Sec. IV A.

A. Computation of the self-trapped electron polaron in AmO_2

It is easy to compute the delocalized state of an excess electron in the supercell (we just add one electron and compute the total energy of the system without performing any structural optimization). But, the computation of the self-trapped electron polaron is more complex. We follow the methodology described in Ref. [40] (hereafter recalled). However, we also have to test among the different possible occupation matrices for the $5f$ orbitals of the Am atom that receives the excess electron.

First, we select one Am atom in the supercell, that will receive the excess electron (and thus will be reduced from Am^{4+} to Am^{3+}). For each of the possible $5f$ occupation matrices of Am^{3+} (there are seven possibilities corresponding to placing six electrons among the seven orbitals of a given spin channel), we use the following two-step procedure:

(1) We first perform a structural optimization with the *5f* occupation matrices on all the Am atoms kept strictly constant along all the electronic self-consistent cycles. The occupation matrix for the *5f* electrons of the Am^{3+} atom (which carries the excess electron) is fixed to one of the seven possibilities mentioned above, while the occupation matrix for the *5f* electrons of the Am^{4+} atoms (all the others) is the one obtained in our previous study [3], i.e., the $M_3^{\text{no sym}}$ matrix. This imposes that the chosen Am atom carries the charge $+3$ while all the other Am carry the charge $+4$, with the $5f$ orbitals occupied according to the imposed matrices, and creates around Am^{3+} the appropriate self-trapping distortion. At the end, the lattice around the polaron has relaxed and is characteristic of a self-trapping distortion able to localize the excess electron on the chosen atom [i.e., a potential similar to that of Fig. 4(b)].

(2) Then, the system is completely optimized without any constraint, starting from the preoptimized geometry obtained just above, and the previous occupation matrices for *5f* orbitals (but maintained only over the 20 first electronic iterations of the first ionic step). This way, the system normally relaxes to a polaronic state with the electron localized on the chosen Am atom, and moreover in the chosen $5f$ orbital (provided this state is stable).

The calculations are performed by switching off all the symmetries. This two-step procedure is achieved for the seven possible occupation matrices of the $5f$ orbitals of the Am^{3+}, and the most stable final configuration is selected as the one that best describes the polaronic state of the excess electron in AmO_2.

In this final configuration, we observe that the added electron is indeed localized on the chosen americium atom (as expected). This localization is associated to (i) an increase of the magnetic moment of the atom on which the electron is localized, from $\sim 5.1\ \mu_B$ up to $5.85\ \mu_B$, and (ii) an expansion of the Am-O bond lengths between the Am^{3+} and its eight oxygen first neighbors, by $\sim 3.3\%$. This increase in the Am-O distances, i.e., the O atoms are slightly pushed away from the localized excess electron, corresponds to the self-trapping distortion characteristic of the polaronic state in AmO_2.

B. Self-trapping energy, formation energy of the electron polaron

The supercell containing the self-trapped electron polaron is 1.01 eV lower in energy than that with a delocalized electron (i.e., at the bottom of the conduction band, in the perfect crystal). The self-trapping energy is thus -1.01 eV. This very large value indicates that electron polarons are extremely stable in AmO_2. This self-trapping energy is larger than the one encountered, e.g., in some rare-earth titanates (-0.55 eV [41]). However, large self-trapping energies may be found, for instance, in $BaCeO_3$, where Swift *et al.* [42] report a self-trapping energy of -0.78 eV for the electron

polaron (which locally corresponds to the reduction of Ce^{4+} in Ce^{3+}). In bulk ceria, however, electron polaron self-trapping energies are less negative (−0.54 to −0.30 eV) [43].

Figure 2 plots the formation energy of the electron polaron as a function of Fermi level, superimposed to the formation energies of oxygen vacancies and Am interstitials. Note that the formation energy of the polaron does not depend on the external conditions.

We observe that, due to its large stability, the formation energy of the electron polaron is positive only over a very small range of the Fermi level near the VBM (between 0 and 0.09 eV). This restricts the accessible range of the Fermi level in AmO_2 to 0–0.09 eV. This is related to the fact that the self-trapping energy of the electron polaron in AmO_2 is very close to the (theoretical) band gap (1.1 eV [3]). Note that a negative value for the formation energy of small polaron would indicate a spontaneous reduction of Am^{4+} to Am^{3+} and, thus, the spontaneous formation of americium sesquioxide Am_2O_3.

The self-trapped electron polaron is therefore a very stable intrinsic defect in AmO_2. In the accessible range of the Fermi level, the dominant atomic point defect is first the fully ionized oxygen vacancy $V_O^{\bullet\bullet}$ (up to $\epsilon_F = 0.01$ eV), then the singly ionized oxygen vacancy $V_O^{\bullet}$. Therefore, in the absence of other point defect in AmO_2, the electron polarons are probably, at least partly charge compensated by fully ionized and partially ionized oxygen vacancies. Note that with a Fermi level so close from the VBM, the AmO_2 matrix can also contain holes, which will be discussed in Sec. VI.

C. Electronic density of states of the polaronic system

Figures 3(a)–3(c) display the electronic density of states (e-DOS) of the supercell containing the self-trapped electron polaron. Figure 3(a) plots the total e-DOS. It can be seen that one occupied state appears in the band gap (it is spotted with green arrow), at very low energy, very close to the VBM, just like the defect states of the neutral oxygen vacancy. Figure 3(b) plots the e-DOS projected on the $5f$ orbitals of the Am^{3+} which carries the excess electron, while Fig. 3(c) plots for comparison the e-DOS projected on the $5f$ orbitals of two Am^{4+} (with opposite spin) of the supercell (their projected e-DOS are typical of those of the other Am^{4+}). Like in the charge-neutral oxygen vacancy (and in bulk AmO_2), the occupied $5f$ orbitals of Am^{4+} are localized down in the valence band [3]. For Am^{3+}, we also observe exactly the same tendency as for the charge-neutral oxygen vacancy: the energy of the newly occupied $5f$ state of Am^{3+} strongly decreases from the CBM down to the VBM, while the energy of the other (occupied) $5f$ states of Am^{3+} increases toward the VBM. As for the oxygen vacancy, Am^{3+} accumulates the occupied $5f$ states at the VBM.

D. Association energy between electron polaron and oxygen vacancy

The large stability of the electron polaron in AmO_2 suggests that the electrons released by an oxygen vacancy may have the tendency to spontaneously unbind from their parent defect, in order to be rather in a self-trapped state, far from the defect in the lattice. We examine this possibility in this section. Having computed the oxygen vacancy in its different possible charge states and the self-trapped electron polaron, we can indeed calculate the association energy between the electron polaron and the oxygen vacancy.

We consider the following processes:

(i) Association between an electron polaron and a singly ionized oxygen vacancy, providing a neutral oxygen vacancy:

$$\underbrace{V_O^{\bullet}}_{\substack{\text{partially ionized}\\ \text{vacancy}}} + \underbrace{Am'_{Am}}_{\substack{\text{isolated small}\\ \text{polaron}}} \rightarrow Am_{Am}^{X} + \underbrace{V_O^{X}}_{\substack{\text{neutral oxygen}\\ \text{vacancy}}} . \qquad (13)$$

We note as E_{a_1} the energy of this process.

(ii) Association between two electron polarons and a fully ionized oxygen vacancy, providing a neutral oxygen vacancy:

$$\underbrace{V_O^{\bullet\bullet}}_{\substack{\text{fully ionized}\\ \text{vacancy}}} + \underbrace{2Am'_{Am}}_{\substack{\text{2 isolated}\\ \text{small polarons}}} \rightarrow 2Am_{Am}^{X} + \underbrace{V_O^{X}}_{\substack{\text{oxygen}\\ \text{vacancy}}} . \qquad (14)$$

We note as E_{a_2} the energy of this process.

$-E_{a_1}$ (respectively $-E_{a_2}$) is thus the energy required to unbind one (respectively two) electron(s) from the neutral vacancy V_O^X and put it (them) far away in the lattice under the form of an (respectively two) isolated self-trapped electron polaron(s), leaving behind a partially (respectively fully) ionized $V_O^{\bullet}$ (respectively $V_O^{\bullet\bullet}$). We find two positives values $E_{a_1} = 0.20$ eV and $E_{a_2} = 0.12$ eV, confirming the larger stability of the polaronic state, i.e., the electron released by the vacancy is more stable far from the vacancy as a self-trapped polaron, rather than bonded to the vacancy (in its close vicinity). In other words, the charge-neutral vacancy is never stable. This is consistent with the fact charged oxygen vacancies are more stable than the neutral one over the accessible range of the Fermi level (Fig. 2).

Other defects are reported in the literature to have the released electrons or holes preferentially localized not on their nearest neighbors: for instance, the electrons liberated by the neutral oxygen vacancy at the $CeO_2(111)$ surface rather localize on next-nearest-neighbor Ce atoms rather than nearest neighbors [44,45]. In bulk ceria, however, electron polarons are found to effectively bind to oxygen vacancies, however weakly, with association energies ~ -0.1 eV [43]. In some perovskites such as $BaZrO_3$ or $BaSnO_3$ doped with trivalent elements on their B site (Zr or Sn), the hole liberated by the acceptor dopant is found to localize on one oxygen second neighbor of the dopant in the case of the largest dopants [40,46].

E. Transfer of the electron polaron

We now investigate the possibility for the electron polaron to migrate from an Am atom onto the nearest one. We denote as Am_i (respectively Am_f) the americium atom on which the electron polaron is initially (respectively finally) localized. The two atoms chosen are first neighbors on the Am sublattice, and carry the same spin (we recall that AmO_2 is modeled as an AFM compound). The basic concepts that underlie the physics of small polaron transfer have been recalled above (Sec. IV B): the hopping of a small polaron is a quantum mechanism taking place in a coincidence configuration, which may appear due to the thermal fluctuations of the lattice atoms.

In a coincidence configuration, the ground levels of the excess electron, considered as localized either in the initial or in the final well, are equalized, making possible a resonant tunneling of the electron from one of these (diabatic) ground states onto the other.

As we have said above, it is generally admitted that, in small polaron transfer, there is mostly one coincidence configuration that contributes to hopping, although in theory, the number of coincidence configurations is infinite, and that this configuration is the lowest-energy one [37]. Along the hopping path, this CC plays the role of the transition state, while its energy E_c (coincidence energy) plays the role of an activation energy for the hopping process of the polaron. It has been proposed to obtain this CC by linear interpolation between the initial and the final self-trapped configurations, and plotting the total energy of the system along this path [47]. This, however, may slightly overestimate the coincidence energy. On the other hand, it is possible to use methods such as the "nudged elastic band" (NEB) or the "string method," which allow computing the minimum energy path (MEP) between the two self-trapped configurations. Note, however, that these techniques assume that the energy evolves smoothly enough along the path: the energy profile must be derivable at the coincidence point, which is the case only if the electronic coupling at coincidence is large enough (see Fig. 5). In theory, this excludes the hopping processes in which the electronic coupling is very weak, i.e., the nonadiabatic processes.

It is, however, difficult to predict by advance the nature (adiabatic or not) of the hopping. Thus, we assume the validity of the string-method algorithm for the present problem, and use it to compute the MEP between two self-trapped configurations corresponding to the polaron localized on neighboring Am sites (with same spin). In the string method, the path between the initial and the final configurations is discretized in a series of intermediate configurations (or images). Initialization is achieved by a linear interpolation, and we use 11 images to make the calculation (including the initial and final ones). The string method is an iterative algorithm in which each iteration consists of two steps: (i) an evolution step, during which the images are moved along the atomic forces computed by a ground-state DFT calculation on each image; (ii) a reparametrization step, during which the images are equally redistributed along the path so that the distance between image k and $k+1$ is constant along the "string." Along the final path, the index of the image is thus proportional to the distance, and thus can be considered as a good reaction coordinate.

At the end of our calculation, the average difference per image between two successive iterations is $\sim 2.0 \times 10^{-4}$ Ha ($\sim$5 meV). The occupation matrices of the $5f$ orbitals are imposed, for each image, over 20 electronic steps at the initial iteration of the string method. For the nine images intermediate between the initial and the final self-trapped configuration, a linear interpolation between the occupation matrices of the two self-trapped configurations is used, as implemented in the ABINIT code [40].

Figure 6 displays the energy profile obtained, as a function of image index: the energy barrier is $\sim$0.55 eV. Along the hopping path, the spin magnetic moments on the initial and final Am show a discontinuous behavior [Fig. 7(b)], transiting suddenly from their initial value ($\sim 5.85\,\mu_B$ for Am_i, $\sim 5.1\,\mu_B$ for Am_f) to their final one ($\sim 5.1\,\mu_B$ for Am_i, $\sim 5.85\,\mu_B$ for Am_f), between images 5 and 6. We recall that $5.85\,\mu_B$ (respectively $5.1\,\mu_B$) is a magnetic moment characteristic of Am^{3+} (respectively Am^{4+}). This means that the electron itself is *abruptly transferred* from Am_i onto Am_f.

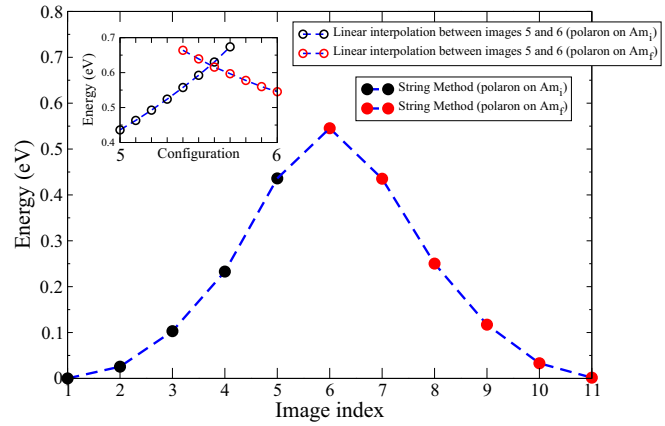

FIG. 6. Energy along the hopping path of the self-trapped polaron, as provided by the string method. Hopping is considered here between two first-neighbor Am atoms. The black (respectively red) part of the curve gathers the configurations in which the polaron is localized on Am_i (respectively Am_f). Inset: energy as a function of configuration linearly interpolated between images 5 and 6 (black symbols: configurations in which the polaron is localized on Am_i; red symbols: configuration in which the polaron is localized on Am_f). Configuration number 1 (respectively 11) is the self-trapped configuration at site Am_i (respectively Am_f).

In order to show how the self-trapping distortion is transferred along the hopping path, we now scrutinize the evolution of the Am_i-O and Am_f-O distances (between $\mathrm{Am}_i/\mathrm{Am}_f$ and the eight first-neighbor oxygens of the first coordination shell, averaged over the eight oxygens), and plot these mean distances as a function of image index along the hopping path [Fig. 7(a)]: we observe that the system undergoes a progressive weakening of the self-trapping distortion in the initial site, and a progressive strengthening of the self-trapping distortion in the final site: indeed, the $\langle \mathrm{Am}_i\text{-O} \rangle$ distance progressively decreases from $\sim$2.43 Å to the undistorted value 2.35 Å, while at the same time, there is a progressive increase of this distance in the final site $\langle \mathrm{Am}_f\text{-O} \rangle$. In the coincidence state, that should be reached somewhere between image 5 and 6, the $\langle$Am-O$\rangle$ distances should be equal to 2.39–2.40 Å in both sites. The CC corresponds to a state in which the distortion is equally shared between the two Am atoms. The self-trapping distortion is therefore *continuously transferred* along the hopping path, in contrast to the electron itself.

Finally, we construct a set of atomic configurations to approach as much as possible the coincidence configuration (CC) involved in the hopping path. For that, we take the two configurations of the path which surround the CC (from Fig. 7, configurations number 5 and 6), and linearly interpolate these two configurations, building 9 intermediate configurations. Then, two series of calculations are performed: the total energy of each of these configurations is computed, with the

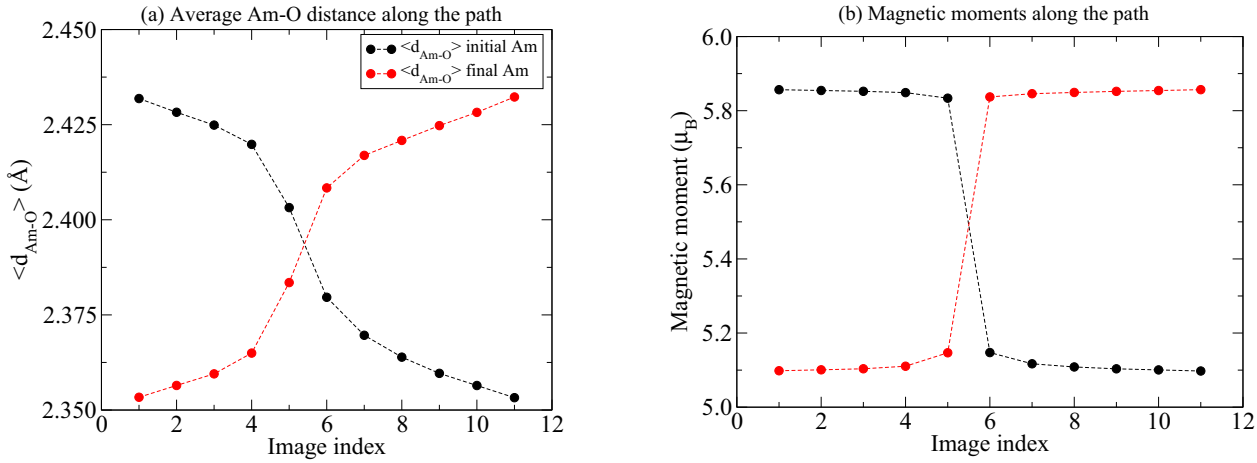

FIG. 7. (a) Evolution of the average distance between the initial (or final) Am and the eight oxygen atoms of the first coordination shell, as a function of image index along the hopping path onto a first- neighbor Am atom. The oxygen atoms are pushed away from the Am^{3+} ion by about 0.08 Å (on average) in the self-trapped state, which is a hallmark of the self-trapping distortion. Here, we see that the self-trapping distortion is progressively transferred from the initial Am onto the final Am along the hopping path of the polaron. (b) Evolution of the magnetic moments of the initial and final Am atoms along the hopping path. Black (respectively red) circles correspond to configurations in which the polaron is localized on Am_i (respectively Am_f).

$5f$ occupation matrices initialized either to those of image 5, or to those of image 6 (which corresponds to initialize the electronic loop with the polaron either on Am_i or on Am_f).

The results are shown in the inset of Fig. 6. The crossing of these two curves provides a better approximation of the CC involved in the hopping. Its energy is ∼0.6 eV above that of the self-trapped configuration. In all these configurations, intermediate between configurations 5 and 6 and close to the CC, the polaron is always obtained as strictly localized on one side of the barrier, i.e., either on Am_i or on Am_f, according to how the calculation is initialized. The calculation does never evolve spontaneously to a state in which the excess electron would be equally shared between Am_i and Am_f, as it could be expected in an adiabatic hopping. Only a small decrease (respectively increase) of the magnetic moment on the polaronic (respectively neighboring) site to ∼5.8 (respectively 5.2) μ_B is observed. The smallest energy difference between the state found localized on Am_i and that found localized on Am_f (reached at the configuration number 7 of the inset of Fig. 6) provides an upper limit to the electronic coupling, namely, $C < 7.2$ meV, because (unconstrained) DFT is not expected to provide diabatic states, but only adiabatic states. The curves of Fig. 6 (with inset) are thus expected to correspond to the solid line curves of Fig. 5. The electronic coupling in the CC is thus probably very weak, providing here the picture of a nonadiabatic hopping.

Having an upper limit to the electronic coupling ($C <$ 7.2 meV), we can estimate an upper limit to the adiabaticity criterion given by Eq. (12). We take as typical phonon energies 0.000 86–0.0026 Hartrees (wave numbers ∼189–570 cm^{-1}) corresponding to the range of the zone-center modes computed in AmO_2 and involving only oxygen displacements (see Appendix). At room temperature, we obtain $\gamma_{th} <$ ∼0.03–0.10, which provides further indication that the hopping probably rather takes place in the nonadiabatic limit.

The transfer barrier of 0.6 eV found here is noticeably larger than polaronic transfer barriers reported in the literature for other oxide compounds, for instance, 0.4 eV [48] or 0.12–0.23 eV [43] in CeO_2 and ∼0.3 eV in $BaCeO_3$ [42] for electron polarons, or ∼0.1–0.2 eV for oxygen-type hole polarons in several oxides [40,46,47], 0.15–0.30 eV for Fe^{3+} holes in $LiFePO_4$ [49–52]. We note that a barrier of 0.5–0.6 eV is reported for hole polarons in TiO_2 in the case of a nonadiabatic hopping [47,53]. The high barrier found here is probably related to the large self-trapping energy of the electron polaron in AmO_2.

A posteriori, we can question the validity of the string-method algorithm on such a mechanism, along which the energy appears as not very smooth at the CC. However, the method provides a continuous path (in the sense of the lattice distortions) between the two self-trapped configurations, with an activation energy smaller than what would be provided by a simple linear interpolation between these two configurations (the linear interpolation provides an activation energy of 0.97 eV). It is thus clearly an improvement over this latter approach.

VI. DISCUSSION

The previous results allow to build the following scenario for AmO_2: the large stability of the electron polaron (which is related to the easiness for Am^{4+} to be reduced into Am^{3+}) restricts the range of possible Fermi levels to a very narrow interval just above the VBM (0–0.09 eV). Electron polarons will be thus in large number in AmO_2, and it is probable that they will be mostly charge compensated by ionized oxygen vacancies (moreover, we have seen that oxygen vacancies spontaneously liberate electron polarons in the lattice). However, since the Fermi level is thus very close to the VBM, we must also consider the possibility to have free holes in addition to the oxygen vacancies to ensure charge compensation of the electron polarons.

We set up a simple and approximate model in order to estimate the concentration in the different defects, charges,

and equilibrium Fermi level [54]. The concentration of free holes is assumed to be

$$p = \int_{-\infty}^{E_{\mathrm{VBM}}} n_v(E) f_p(E) dE, \tag{15}$$

with

$$n_v(E) = \frac{1}{2\pi^2}\left\{\frac{2m_h^*}{\hbar^2}\right\}^{3/2}\sqrt{E_{\mathrm{VBM}} - E} \tag{16}$$

and $f_p(E) = \frac{1}{1+e^{-(E-\mu_e)/k_BT}}$. The concentration of free (band) electrons is neglected since electrons in the lattice clearly prefer the polaronic state. For simplicity, we take the effective mass m_h^* equal to the electron mass [55]. The concentration of point defect X in charge state q is

$$[X^q] = [M] e^{-\frac{\Delta E_f(X,q)}{k_BT}}, \tag{17}$$

with $[M]$ being the concentration in possible sites for the defect (e.g., for V_{O} this is the oxygen concentration in AmO_2) [36]. The formation energy of the defect, $\Delta E_f(X, q)$, depends on the oxygen chemical potential $\Delta\mu_{\mathrm{O}}$ (external conditions) and on the Fermi level ϵ_F if $q \neq 0$.

The Fermi level at equilibrium ϵ_F^{eq} may be obtained by solving the electroneutrality equation, assuming that oxygen vacancies are the only atomic defects in the system (with possible charge states 2+, 1+, 0):

$$[e^-_{\mathrm{pol}}] = p + 2\left[V_{\mathrm{O}}^{2+}\right] + \left[V_{\mathrm{O}}^{1+}\right], \tag{18}$$

where $[e^-_{\mathrm{pol}}]$ denotes the concentration of electron polarons. Numerical applications are done here for $T = 300$ K. Note that Eq. (18) is solved for a given value of $\Delta\mu_{\mathrm{O}}$ (which acts as a parameter).

Equation (18) admits positive solutions (i.e., ϵ_F^{eq} remains in the band gap) only for oxygen-poor conditions. Using $\Delta\mu_{\mathrm{O}} = -0.75$ eV, we obtain $\epsilon_F^{\mathrm{eq}} = 0.012\,314$ eV. In these conditions, the concentration of electron polarons is $\sim$0.059 per f.u., that of free holes $\sim 5.2 \times 10^{-4}$ per f.u., and that of oxygen vacancies, 0.040 per f.u. This means that almost 6% of the Am atoms in AmO_2 are spontaneously reduced into Am^{3+} under such external conditions. We see that the electron polarons are mostly compensated by the oxygen vacancies rather than by the holes, and that the concentration of oxygen vacancies is significant, leading for AmO_2 to the picture of a nonstoichiometric compound, with formula $AmO_{1.96}$ (for $T = 300$ K and $\Delta\mu_O = -0.75$ eV). With an equilibrium Fermi level so close to the VBM, the concentration of free holes is significant, but is dominated by that of electron polarons by about two orders of magnitude, at least for a hole effective mass equal to the free-electron mass. If a larger hole mass is assumed, e.g., 10 times that of free electron, we have $\epsilon_F^{\mathrm{eq}} = 0.014\,845$ eV and the concentration in oxygen vacancies slightly decreases to $\sim$3.5%. Then, the concentration in free holes is increased, although remaining $\sim$4 times smaller than that of electron polarons. The important loss of oxygen in those oxygen-poor conditions may be seen as precursor for the formation of hypostoichiometric Am oxide.

Note, however, that the very large concentrations found here (due to very small formation energies) make the present defect model very approximate since the calculation of the concentration based on the formation energy normally assumes concentrations $\ll 1$.

In oxygen-rich conditions ($\Delta\mu_{\mathrm{O}} = -0.29$ eV), the formation energy of the oxygen vacancy becomes too large to allow charge compensation of the electron polarons by $V_{\mathrm{O}}^{\bullet\bullet}$ or $V_{\mathrm{O}}^{\bullet}$, and this role is probably entirely played by free holes. There is probably no important loss of oxygen in those conditions.

VII. CONCLUSION

In this work, we have studied intrinsic donor point defects and electron polarons in AmO_2, using a first-principles GGA + U framework within which the Am $5f$ orbital occupation matrices are carefully controlled. We have shown that the oxygen vacancy is a deep double donor, with small to moderate formation energies. Americium interstitials have prohibitive formation energies and are thus unlikely in AmO_2. The self-trapped electron polaron is extremely stable (self-trapping energy -1.01 eV). This large stability confines the possible values of the Fermi level in AmO_2 to a very narrow interval just above the valence band maximum (0–0.09 eV).

In the oxygen-poor conditions here considered ($\Delta\mu_{\mathrm{O}} = -0.75$ eV, i.e., $T = 680$ K and $P_{\mathrm{O}_2} = 0.2$ atm), oxygen vacancies are easily formed in AmO_2. The liberated electrons have the tendency to move far from the vacancies and localize in the lattice under the form of self-trapped polarons since this state is found more stable than when the electron is trapped close to the vacancy. In other words, the oxygen vacancies are spontaneously ionized. Electron polarons are probably in rather large number, with charge compensation mostly ensured by ionized and partially ionized oxygen vacancies. In oxygen-rich conditions, electron polarons may remain in large concentration but should be charge compensated by free holes rather than by ionized oxygen vacancies.

The self-trapped state of the excess electron in AmO_2 is associated with a self-trapping distortion mostly consisting of an increase of the Am-O distance (between Am carrying the excess electron and the eight first-neighbor oxygens) by about 0.08 Å. The hopping of the polaron involves a rather large activation barrier of $\sim$0.6 eV, and probably takes place by a nonadiabatic mechanism.

ACKNOWLEDGMENTS

This work was performed using high-performance computing resources from Grand Equipement National de Calcul Intensif (GENCI) [Très Grand Centre de Calcul (TGCC) and Centre Informatique National de l'Enseignement Supérieur (CINES)]. This research is part of the INSPYRE project (Investigations Supporting MOX Fuel Licensing in ESNII Prototype Reactors), which has received funding from Euratom research and training programme 2014–2018 under Grant No. 754329.

APPENDIX: PHONON MODES AT THE Γ POINT IN AmO_2

The phonon modes at the Γ point in AmO_2 have been computed using a finite-difference (frozen-phonon) method, in a six-atom supercell (to allow 1k antiferromagnetism), optimized without symmetry constraint to reach the GGA + U

ground state [3]. The occupation matrix for the $5f$ correlated orbitals is the one called $M_3^{\text{no sym}}$ in Ref. [3]. Note that the structural optimization within GGA + U without symmetry constraint provides a unit cell which is slightly distorted from the ideal fluorite cell, which explains why the computed phonon modes are nondegenerate. The phonon wave numbers obtained, using for Am a mass of 241 a.m.u. (and excluding the three zero-frequency acoustic modes) are 114.3, 116.5, 188.6, 189.3, 230.5, 238.3, 305.2, 317.6, 320.7, 424.2, 425.2, 453.4, 454.2, 463.8, and 570.4 cm^{-1}. Among these modes, the first one involving only oxygen displacements is the one at 189.3 cm^{-1}.

[1] R. O'Brien, R. Ambrosi, N. Bannister, S. Howe, and H. V. Atkinson, J. Nucl. Mater. **377**, 506 (2008).

[2] L. Summerer and K. Stephenson, in *Proceedings of the Institution of Mechanical Engineers*, Part G: Journal of Aerospace Engineering (Sage Publications, London, UK, 2011), Vol. 225, p. 129.

[3] M. S. Talla Noutack, G. Geneste, G. Jomard, and M. Freyss, Phys. Rev. Mater. **3**, 035001 (2019).

[4] X. D. Wen, R. L. Martin, L. E. Roy, G. E. Scuseria, S. P. Rudin, E. R. Batista, T. M. McCleskey, B. L. Scott, E. Bauer, J. J. Joyce, and T. Durakiewicz, J. Chem. Phys. **137**, 154707 (2012).

[5] C. Suzuki, T. Nishi, M. Nakada, M. Akabori, M. Hirata, and Y. Kaji, J. Phys. Chem. Solids **73**, 209 (2012).

[6] L. Petit, A. Svane, Z. Szotek, W. M. Temmerman, and G. M. Stocks, Phys. Rev. B **81**, 045108 (2010).

[7] A. Jankowiak, C. Maillard, and L. Donnet, J. Nucl. Mater. **393**, 87 (2009).

[8] M. Takano, M. Akabori, Y. Arai, and K. Minato, J. Nucl. Mater. **376**, 114 (2008).

[9] C. Hurtgen and J. Fuger, Inorg. Nucl. Chem. Lett. **13**, 179 (1977).

[10] R. Ewing, W. Weber, and F. Clinard, Jr., Prog. Nucl. Energy **29**, 63 (1995).

[11] D. Prieur, J.-F. Vigier, T. Wiss, A. Janssen, J. Rothe, A. Cambriani, and J. Somers, J. Solid State Chem. **212**, 7 (2014).

[12] D. Staicu, T. Wiss, V. Rondinella, J. Hiernaut, R. Konings, and C. Ronchi, J. Nucl. Mater. **397**, 8 (2010).

[13] P. Gotcu-Freis, J.-Y. Colle, C. Guéneau, N. Dupin, B. Sundman, and R. Konings, J. Nucl. Mater. **414**, 408 (2011).

[14] E. Epifano, C. Guéneau, R. C. Belin, R. Vauchy, F. Lebreton, J.-C. Richaud, A. Joly, C. Valot, and P. M. Martin, Inorg. Chem. **56**, 7416 (2017).

[15] M. W. Chase, Jr., C. A. Davies, J. R. Downey, Jr., D. J. Frurip, R. A. McDonald, and A. N. Syverud, *JANAF Thermochemical Tables*, 3rd ed., Journal of Physical and Chemical Reference Data, Vol. 14, Suppl. 1 (American Chemical Society, Washington, 1985).

[16] T. R. Paudel, S. S. Jaswal, and E. Y. Tsymbal, Phys. Rev. B **85**, 104409 (2012).

[17] T. Chikalla and L. Eyring, J. Inorg. Nucl. Chem. **30**, 133 (1968).

[18] G. Makov and M. C. Payne, Phys. Rev. B **51**, 4014 (1995).

[19] A. Zywietz, J. Furthmüller, and F. Bechstedt, Phys. Rev. B **59**, 15166 (1999).

[20] Y. Yao and H. Fu, Phys. Rev. B **84**, 064112 (2011).

[21] P. G. Sundell, M. E. Björketun, and G. Wahnström, Phys. Rev. B **73**, 104112 (2006).

[22] X. Gonze, J.-M. Beuken, R. Caracas, F. Detraux, M. Fuchs, G.-M. Rignanese, L. Sindic, M. Verstraete, G. Zerah, F. Jollet *et al.*, Comput. Mater. Sci. **25**, 478 (2002).

[23] X. Gonze, G.-M. Rignanese, M. Verstraete, J.-M. Beuken, Y. Pouillon, R. Caracas, F. Jollet, M. Torrent, G. Zerah, M. Mikami, Ph. Ghosez, M. Veithen, J.-Y. Raty, V. Olevano, F. Bruneval, L. Reining, R. Godby, G. Onida, D. R. Hamann,and D. C. Allan, Z. Kristallogr. **220**, 558 (2005).

[24] P. E. Blöchl, Phys. Rev. B **50**, 17953 (1994).

[25] M. Torrent, F. Jollet, F. Bottin, G. Zérah, and X. Gonze, Comput. Mater. Sci. **42**, 337 (2008).

[26] J. P. Perdew, K. Burke, and M. Ernzerhof, Phys. Rev. Lett. **77**, 3865 (1996).

[27] V. I. Anisimov, J. Zaanen, and O. K. Andersen, Phys. Rev. B **44**, 943 (1991).

[28] A. I. Lichtenstein and M. I. Katsnelson, Phys. Rev. B **57**, 6884 (1998).

[29] A. I. Liechtenstein, V. I. Anisimov, and J. Zaanen, Phys. Rev. B **52**, R5467(R) (1995).

[30] B. Amadon, F. Jollet, and M. Torrent, Phys. Rev. B **77**, 155104 (2008).

[31] H. J. Monkhorst and J. D. Pack, Phys. Rev. B **13**, 5188 (1976).

[32] G. Jomard, B. Amadon, F. Bottin, and M. Torrent, Phys. Rev. B **78**, 075125 (2008).

[33] L. Shi, Etude par calcul de structure électronique des dioxydes d'uranium et de cérium contenant des défauts et des impuretés, Ph.D. thesis, Université Aix-Marseille, 2016.

[34] R. J. Konings, O. Beneš, A. Kovács, D. Manara, D. Sedmidubský, L. Gorokhov, V. S. Iorish, V. Yungman, E. Shenyavskaya, and E. Osina, J. Phys. Chem. Ref. Data **43**, 013101 (2014).

[35] Y. Lu, Y. Yang, F. Zheng, B.-T. Wang, and P. Zhang, J. Nucl. Mater. **441**, 411 (2013).

[36] C. G. Van de Walle and A. Janotti, Advances in electronic structure methods for defects and impurities in solids, in *Advanced Calculations for Defects in Materials*, edited by A. Alkauskas, P. Deák, J. Neugebauer, A. Pasquarello, and C. G. Van de Walle (Wiley, Weinheim, 2011).

[37] A. Shluger and A. Stoneham, J. Phys.: Condens. Matter **5**, 3049 (1993).

[38] F. Wu and Y. Ping, J. Mat. Chem. A **6**, 20025 (2018).

[39] A. Staib, D. Borgis, and J. T. Hynes, J. Chem. Phys. **102**, 2487 (1995).

[40] G. Geneste, B. Amadon, M. Torrent, and G. Dezanneau, Phys. Rev. B **96**, 134123 (2017).

[41] L. Bjaalie, D. Ouellette, P. Moetakef, T. Cain, A. Janotti, B. Himmetoglu, S. Allen, S. Stemmer, and C. Van de Walle, Appl. Phys. Lett. **106**, 232103 (2015).

[42] M. Swift, A. Janotti, and C. G. Van de Walle, Phys. Rev. B **92**, 214114 (2015).

[43] L. Sun, X. Huang, L. Wang, and A. Janotti, Phys. Rev. B **95**, 245101 (2017).

[44] M. V. Ganduglia-Pirovano, J. L. F. Da Silva, and J. Sauer, Phys. Rev. Lett. **102**, 026101 (2009).

[45] H.-Y. Li, H.-F. Wang, X.-Q. Gong, Y.-L. Guo, Y. Guo, G. Lu, and P. Hu, Phys. Rev. B **79**, 193401 (2009).

[46] A. Lindman, P. Erhart, and G. Wahnström, Phys. Rev. B **94**, 075204 (2016).
[47] N. A. Deskins and M. Dupuis, Phys. Rev. B **75**, 195212 (2007).
[48] J. J. Plata, A. M. Márquez, and J. F. Sanz, J. Phys. Chem. C **117**, 25497 (2013).
[49] S. P. Ong, V. L. Chevrier, and G. Ceder, Phys. Rev. B **83**, 075112 (2011).
[50] M. D. Johannes, K. Hoang, J. L. Allen, and K. Gaskell, Phys. Rev. B **85**, 115106 (2012).
[51] T. Maxisch, F. Zhou, and G. Ceder, Phys. Rev. B **73**, 104301 (2006).
[52] K. Hoang and M. Johannes, Chem. Mater. **23**, 3003 (2011).
[53] N. A. Deskins, R. Rousseau, and M. Dupuis, J. Phys. Chem. C **113**, 14583 (2009).
[54] V. Kosyak, N. Mortazavi Amiri, A. Postnikov, and M. Scarpulla, J. Appl. Phys. **114**, 124501 (2013).
[55] Approximating the e-DOS of perfect AmO_2 close to the VBM by Eq. (16) is good down to 0.2 eV below the VBM. An estimation of the hole effective mass based on a fit of the e-DOS by Eq. (16) close to the VBM leads to $m_h^* \approx 1.4$ electron mass.